SANDIA REPORT

SAND2003-3156
Unlimited Release
Printed October 2003

Preliminary Uncertainty and Sensitivity Analysis for Basic Transport Parameters at the Horonobe Site, Hokkaido, Japan

Scott C. James and Dean A. Zimmerman

Prepared by
Sandia National Laboratories
Albuquerque, New Mexico 87185 and Livermore, California 94550

Sandia is a multiprogram laboratory operated by Sandia Corporation,
a Lockheed Martin Company, for the United States Department of Energy's
National Nuclear Security Administration under Contract DE-AC04-94AL85000.

Issued by Sandia National Laboratories, operated for the United States Department of Energy by Sandia Corporation.

Available to DOE and DOE contractors from
U.S. Department of Energy
Office of Scientific and Technical Information
P.O. Box 62
Oak Ridge, TN 37831

Telephone: (865) 576-8401
Facsimile: (865) 576-5728
E-Mail: reports@adonis.osti.gov
Online order: http://www.doe.gov/bridge

Available to the public from
U.S. Department of Commerce
National Technical Information Service
5285 Port Royal Rd
Springfield, VA 22161

Telephone: (800) 553-6847
Facsimile: (703) 605-6900
E-Mail: orders@ntis.fedworld.gov
Online order: http://www.ntis.gov/help/ordermethods.asp?loc=7-4-0#online

SAND2003-3156
Unlimited Release
Printed October 2003

Preliminary Uncertainty and Sensitivity Analysis for Basic Transport Parameters at the Horonobe Site, Hokkaido, Japan

Scott C. James
Geohydrology Department
Sandia National Laboratories
P.O. Box 5800
Albuquerque, New Mexico 87185-0735
scjames@sandia.gov

Dean A. Zimmerman
Gram Incorporated
Albuquerque, NM 87112
dazimme@sandia.gov

Abstract: Incorporating results from a previously developed finite element model, an uncertainty and parameter sensitivity analysis was conducted using preliminary site-specific data from Horonobe, Japan (data available from five boreholes as of 2003). Latin Hypercube Sampling was used to draw random parameter values from the site-specific measured, or approximated, physicochemical uncertainty distributions. Using pathlengths and groundwater velocities extracted from the three-dimensional, finite element flow and particle tracking model, breakthrough curves for multiple realizations were calculated with the semi-analytical, one-dimensional, multirate transport code, STAMMT-L. A stepwise linear regression analysis using the 5, 50, and 95% breakthrough times as the dependent variables and LHS sampled site physicochemical parameters as the independent variables was used to perform a sensitivity analysis. Results indicate that the distribution coefficients and hydraulic conductivities are the parameters responsible for most of the variation among simulated breakthrough times. This suggests that researchers and data collectors at the Horonobe site should focus on accurately assessing these parameters and quantifying their uncertainty. Because the Horonobe Underground Research Laboratory is in an early phase of its development, this work should be considered as a first step toward an integration of uncertainty and sensitivity analyses with decision analysis.

TABLE of CONTENTS

LIST of FIGURES

LIST of TABLES

Introduction

The Japan Nuclear Cycle Development Institute (JNC) is undertaking geologic investigations at Horonobe, in northwestern Hokkaido, for the potential development of an underground research laboratory (URL) for research into geologic disposal of high-level radioactive wastes in sedimentary host rocks. The proposed Horonobe URL will be constructed at a depth of approximately 500 m in a basinal Tertiary mudstone sequence up to 1,000 m thick (BGS, 2002). The proposed research and development programs include geologic and hydrochemical investigations of the deep geologic environment, developing techniques for planning and constructing repository facilities, and developing methodologies to conduct performance assessment (PA) modeling for the site. The study will be divided into three stages as follows and will conclude after about 20 years:

> Stage 1: Research activities directed from the ground surface including borehole investigations (for up to six years).
>
> Stage 2: Research activities in excavated tunnels (for up to six years).
>
> Stage 3: Research activities using specially excavated experimental galleries (for 9 to 11 years).

Stage 1 of the investigations began in 2001. In March 2002, JNC completed the drilling of two fully cored deep boreholes (HDB-1 and HDB-2) to depths of 720 m. A series of three shallower boreholes to depths of 520 m were completed in late 2002 (HDB-3, HDB-4, and HDB-5).

In Japanese fiscal year H14 (April 1, 2002-March 31, 2003), Sandia National Laboratories (SNL) was asked to perform an uncertainty and sensitivity analysis on geologic and geochemical parameters affecting the transport of radionuclides of interest at the Horonobe URL. To date, JNC has completed five boreholes and five additional boreholes are in the planning phase. The goal of the uncertainty and sensitivity analysis is to help direct site characterization efforts for the remaining boreholes. Specifically, the analysis identifies the most important physicochemical parameters to be sampled. An important parameter is defined as one with either significant impact upon model performance (results), or one where a large uncertainty in its value (or range) translates into a large uncertainty in results. Given the particle tracking data from the available finite element flow model and site-specific borehole data, one-dimensional, dual-porosity, reactive solute transport can be modeled using STAMMT-L (Haggerty and Gorelick, 1995; 1998; Haggerty and Reeves, 1999). The results from this transport model are used in a sensitivity analysis in an attempt to identify and rank the importance of site parameters.

Horonobe staff members have provided SNL with enough borehole data to construct empirical cumulative distribution functions (CDFs) of the uncertainty in porosity, saturation, fracture frequency, grain density, and temperature at each borehole. Although, five important radionuclides were specified for study: Cesium, Neptunium, Selenium, Thorium, and Uranium; in this study, only results pertinent to Np, Th, and U are presented. Unfortunately, distribution coefficients, K_ds, for these radionuclides in Horonobe soils and rocks are not yet available. Therefore, SNL conducted a literature search for distribution coefficients in anoxic media and have selected a distribution of K_d for the studied radionuclides with means equal to the values specified in JNC's H12 report (JNC, 2000).

Although sparse site-specific data are available at the Horonobe URL, preliminary performance assessment modeling should begin. Because site characterization (SC) and PA are expected to evolve together, one guiding the other, it is important to begin uncertainty and sensitivity modeling as soon as data become available. With two deep and three shallow exploratory

boreholes completed at the Horonobe site, and several more under construction, enough information is available to begin the PA modeling process.

STAMMT-L calculates the semi-analytical breakthrough curves for a dual-porosity reactive transport system. SNL has extracted geologic unit travel length and travel time information from the particle tracks (see following section) to be used as STAMMT-L input. Additionally, STAMMT-L requires site-specific information including: porosity, saturation, half matrix block length (fracture frequency), grain density, temperature, and radionuclide distribution coefficients. Sample values for each of these parameters were generated using a Latin Hypercube Sampling (LHS) technique. These randomly sampled data were input to STAMMT-L where a constant concentration source is assumed at the starting location. Although the flow model investigated 12 particle release points, only two are chosen for study, those roughly originating at HDB-1 and HDB-2. STAMMT-L was then run in Monte Carlo fashion to observe the variations in breakthrough response due to changes in the LHS input parameters. Model output reflects the sensitivity of the input parameters. Furthermore, the range of values supplied to STAMMT-L (the uncertainty) define the spread of the breakthrough curves. The spread of the results are related to the uncertainty in the input parameters, thereby identifying which parameters require further characterization by additional field measurements.

The Finite Element Flow Model

In 2002, the Hazama Corporation developed a finite element model for the flow system of the area surrounding proposed site for the Horonobe URL (JNC, 2002). The model domain covers ~2,000 km^2 and comprises 78,000 elements. Model elevations range from 500 m above sea level to 5,000 m below sea level. Boundary conditions include four no flow boundaries (three sides and the bottom), a constant head side boundary due to the ocean, and a free surface on top with 1 mm/day recharge. A schematic of the finite element mesh used is shown in Figure 1. The model comprises 11 distinct geologic units that include two faults (Oomagari and N-Systems Faults), all with a specified porosity of 0.38.

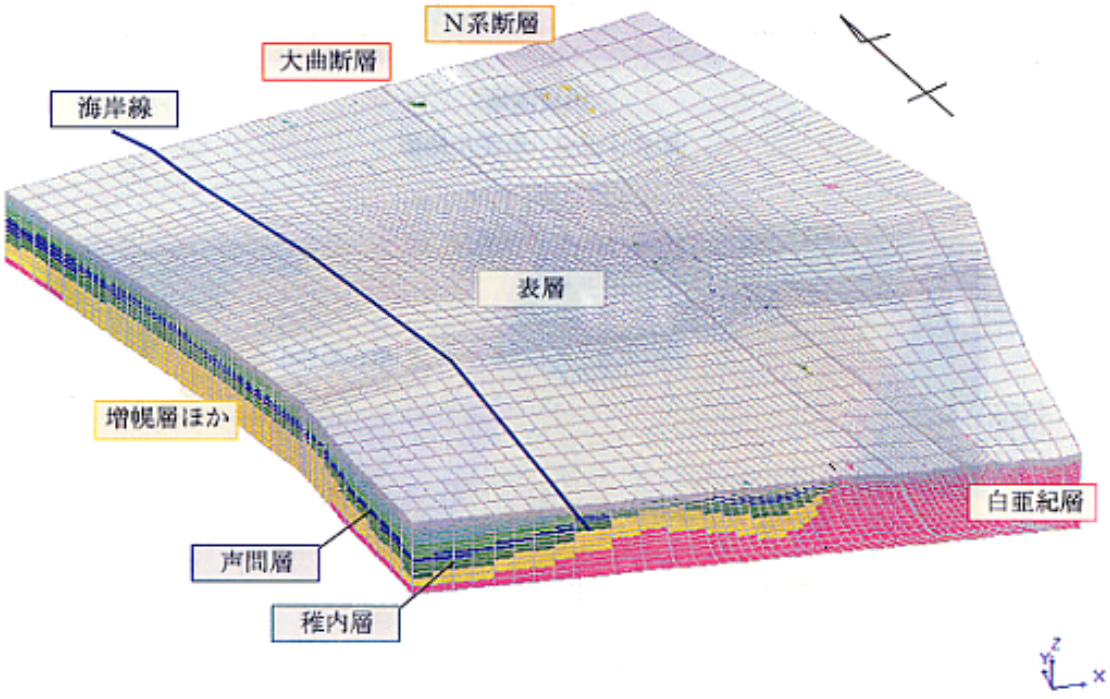

Figure 1: Schematic of the finite element mesh for the flow system model.

A sensitivity analysis has been performed on the flow field as affected by changes in hydraulic conductivity of a single geologic unit. Specifically, particle tracks were calculated for each geologic 'variant.' A variant is defined as an increase or decrease of the hydraulic conductivity, *K*, for a single geologic unit. Although eleven distinct geologic units were defined, only eight of them were altered for variant particle tracking runs. Table 1 lists the base case hydraulic conductivities for each of the eleven geologic units in the flow model along with high and low *K* variants for applicable formations.

Table 1: Geologic unit hydraulic conductivity and corresponding variant information.

Geologic unit	*K* (m/s)	Variant – high *K* (m/s)	Variant – low *K* (m/s)
Cretaceous	10^{-11}		
Mashuhoro (**M**)	5×10^{-10}	3.15×10^{-9}	7.92×10^{-11}
Wakkanai (**W**)	10^{-10}	10^{-9}	10^{-11}
Koitoi (**K**)	10^{-9}	10^{-8}	10^{-10}
Yuuchi (**Y**)	10^{-7}	3.16×10^{-6}	3.16×10^{-9}
Quaternary, Sarobetu (**Q**)	10^{-6}	3.16×10^{-5}	3.16×10^{-8}
Side of Oomagari fault (**SOF**)	10^{-8}	10^{-6}	10^{-10}
Center of Oomagari fault (**COF**)	10^{-10}	10^{-8}	10^{-12}
Side of N System fault	10^{-8}		
Middle of N System fault	10^{-10}		
Surface (**S**)	2×10^{-6}	6.32×10^{-5}	6.32×10^{-8}

Both forward and reverse particle tracking with 12 particles using a constant 200 m spatial step were conducted, although only the forward particle tracks are used in this analysis. These forward particle tracks formed the basis of the uncertainty and sensitivity analysis of radionuclide transport times. Because two of the 12 particle release points correspond to HDB-1 and HDB-2 at a depth of 500 m, these were the two selected for further analysis. Depending on the variant, these particles traveled at different speeds along different paths. Pathlength and velocity data are shown in Table 2

Table 2: Particle transport properties across the 17 variant cases run in the flow model. Particle 5 corresponds to HDB-1 and particle 8 corresponds to HDB-2.

Particle #	Min. dist. (m)	Avg. dist. (m)	Max. dist. (m)	Min. vel. (m/s)	Avg. vel (m/s)	Max. vel. (m/s)
5	2,029	2,652	2,999	1.4×10^{-6}	1.0×10^{-5}	5.9×10^{-5}
8	880	5,003	6,276	4.5×10^{-7}	1.8×10^{-6}	4.4×10^{-6}

STAMMT-L Transport Modeling

Overview of the Model

A one-dimensional, dual porosity, semi-analytical, multirate mass transfer code, STAMMT-L (Haggerty and Gorelick, 1995) was used to preliminarily model radionuclide breakthrough at the Horonobe URL. STAMMT-L provides a semi-analytical solution to the one-dimensional dual-porosity, advective-dispersive transport equation with mass-transfer between the mobile and immobile domains. In keeping with the classic double-porosity model, advection occurs only within the mobile zone (fractures) and the immobile zone (matrix) acts as a storage volume. Mass-transfer between the mobile and immobile domains may be represented as a multirate process (Haggerty, 1999), although this capability is not used in this study. For this system, the mobile zone is conceptualized as the fractured mudstone and shale and the immobile zone is the diatomaceous matrix. Mass transfer processes, such as adsorption and diffusion, control the distribution of radionuclide mass between the two zones. The immobile zone is represented as a domain of prescribed thickness with a characteristic diffusion rate coefficient, or first-order mass transfer rate. Equilibrium sorption of the radionuclides onto the fracture walls as well as onto the porous matrix is assumed. The conceptual model for application of STAMMT-L in a fractured rock system is shown in Figure 2.

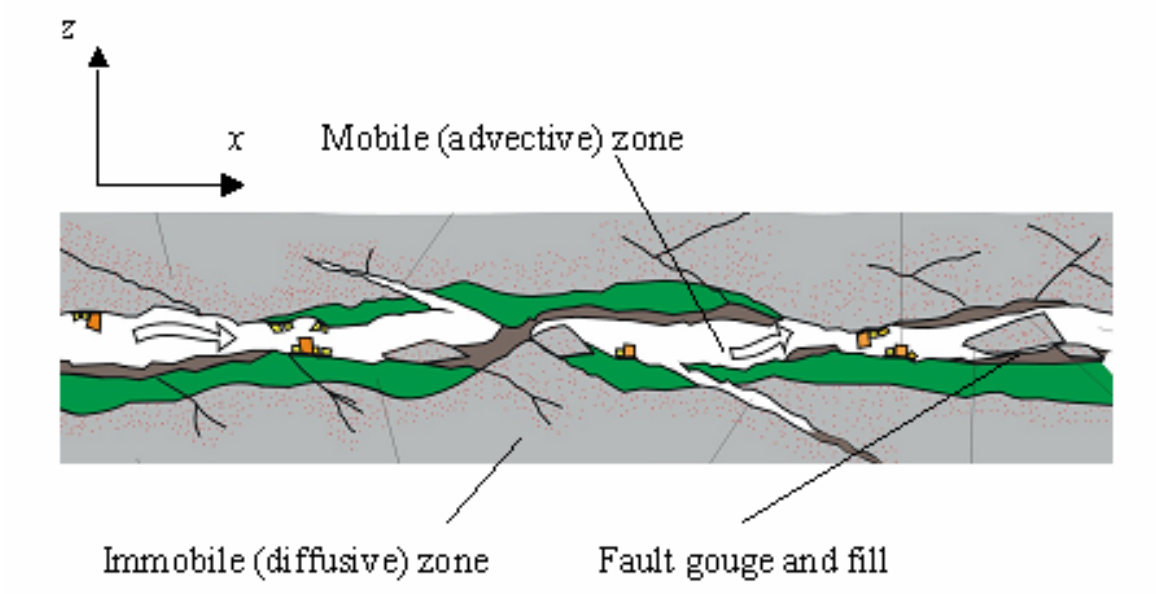

Figure 2: Conceptual model of STAMMT-L where mass transfer takes place between the mobile and immobile zones.

As mentioned above, STAMMT-L can be used to estimate mass transfer rates. A complete description of this model is found in the STAMMT-L User's Manual (Haggerty and Reeves, 1999), as well as in the work of Haggerty and Gorelick (1995; 1998). Versions of STAMMT-L have been used to model transport at the WIPP site (Meigs et al., 1997; Haggerty et al., 2001; McKenna et al., 2001), the Äspö TRUE-1 tracer tests (McKenna, 1999; 2000a;b), as well as for the CRR experiments conducted in Grimsel. Although STAMMT-L is one-dimensional, because pathlengths and travel times come from the three-dimensional flow model, STAMMT-L is, in some respect, quasi-three-dimensional. That is, results from the three-dimensional model are passed along to the one-dimensional model, which calculates radionuclide transport subject to equilibrium reaction with the medium, thereby effectively taking into account three-dimensional flow effects.

Model Development

Advective-dispersive transport in a one-dimensional system, subject to rate-limited mass transfer can be described mathematically as (Haggerty and Gorelick, 1995, eq. 3; Haggerty, 1999, eq. 4-1):

$$\frac{\partial c_m(x,t)}{\partial t} + \beta \frac{\partial \hat{c}_{im}(t;\alpha_d)}{\partial t} = \frac{\alpha_L \overline{v}}{R_m} \frac{\partial^2 c_m(x,t)}{\partial x^2} - \frac{\overline{v}}{R_m} \frac{\partial c_m(x,t)}{\partial x}, \tag{1}$$

where c_m [M/L^3] is concentration in the mobile zone, $\hat{c}_{im}(t;\alpha_d)$ [M/L^3] is the average concentration in the immobile zone subject to diffusion rate α_d [1/T], β [–] is the 'capacity ratio' defined below; α_L [L] is longitudinal dispersivity (dispersion length) of the solute in the mobile zone; $\overline{v}$ [L/T] is mobile zone pore-water (solute) velocity; R_m [–] is the retardation factor of the mobile zone; t [t] is time; and x [L] is distance along the flow path from the injection point.

The upstream and downstream boundary conditions for the preceding transport equation are specified concentration (Dirichlet) at the injection point:

$$c_m(0,t) = c_{inj}(t), \tag{2}$$

and a non-dispersive flux condition (Neumann) at the end of the system (some distance greater than the pathlength)

$$\frac{\partial c_m(L_s,t)}{\partial x} = 0, \tag{3}$$

respectively, where $c_{inj}(t)$ [M/L^3] is the input concentration (unit or normalized); and L_s [L] is the length of the system (in this work, L_s is always twice the pathlength). The initial conditions for the system are that the mobile and immobile zone concentrations are zero, $c_m(x,0) = c_{im}(x,0) = 0$.

The total capacity for mass uptake in the medium is defined as (Haggerty and Gorelick, 1995, eq. 4)

$$\beta = \frac{R_{im}\phi_{im}}{R_m\phi_m}, \tag{4}$$

where R_{im} represents the retardation factor for the immobile (non-advecting) zone, ϕ_m is the porosity in the mobile (advective) zone (porosity of fracture fill – assumed equal to 1 in this work), and ϕ_{im} is the immobile zone porosity. At equilibrium conditions, the concentrations of mass are evenly distributed for a diffusing solute and there is no concentration gradient between the mobile (advective) and immobile (diffusive) zones. For a conservative tracer, the retardation

factor is unity and β is simply the ratio of the immobile to mobile zone porosities: ϕ_{im}/ϕ_m. For the case of a sorbing and diffusing solute, the ratio of mobile to immobile zone concentrations includes the retardation factors.

The diffusion rate coefficient is defined as (McKenna, 1999, eq. 1-3)

$$\alpha_d = \frac{D_{aq}\tau\phi_{im}}{(\phi_{im} + K_d\rho_b)\ell^2}, \tag{5}$$

where D_{aq} [L^2/T] is the aqueous diffusion coefficient; τ [–] is the tortuosity; ℓ [L] is the variable length of the diffusion pathway within the immobile zone or half matrix block length; and the porosity, bulk density, and distribution coefficient of the immobile zone are ϕ_{im} [–], ρ_b [M/L^3], and K_d [L^3/M], respectively. Note that for a non-sorbing tracer, $K_d = 0$, the diffusion rate coefficient reduces to $\alpha_d = D_{aq}\tau/\ell^2$.

The immobile zone concentration subject to a specific diffusion rate coefficient is given by the solution to the diffusion equation:

$$\frac{\partial c_{im}(z,t;\alpha_d)}{\partial t} = \frac{D_{aq}\tau}{R_{im}}\frac{\partial^2 c_{im}(z,t;\alpha_d)}{\partial z^2}, \tag{6}$$

As seen in the preceding equation, immobile zones are assumed mathematically one-dimensional. Essentially, the immobile zone is conceptualized as porous layer with one end in contact with the mobile zone.

The boundary condition at the interface between the immobile and mobile zones is:

$$c_{im}\left(0,t;\alpha_d\right) = c_m\left(X,t\right), \tag{7}$$

where X [L] is the distance from the solute source to the observation location (the observation location in this model is the end of the particle track). No flux is specified at the center of the immobile zone (at the half matrix block length),

$$\frac{\partial c_{im}\left(\ell,t;\alpha_d\right)}{\partial z} = 0, \tag{8}$$

and the immobile zone is initially free of radionuclides, c_{im}(z,0) = 0.

The first-order mass transfer rate between mobile and immobile zones at the observation point (pathlength of the particle tracks) is expressed as

$$\frac{\partial \hat{c}_{im}\left(t;\alpha_d\right)}{\partial t} = \alpha_d\left[c_m\left(X,t\right) - \hat{c}_{im}\left(t;\alpha_d\right)\right], \tag{9}$$

where z [L] is the coordinate along the diffusion pathway and perpendicular to x, and the average solute concentration along a specific diffusion pathway in the immobile zone is:

$$\hat{c}_{im}(t;\alpha_d) = \frac{1}{\ell}\int_0^{\ell} c_{im}(z,t;\alpha_d)\,\mathrm{d}z. \tag{10}$$

It should be noted that STAMMT-L yields the time dependent solute concentration at a specified location along the flow path, hence the use of X in (9). Once the time rate of change of average radionuclide concentration in the immobile zone has been calculated according to (9), it is substituted into (1) to yield the overall solution for mobile radionuclide concentration.

Parameters

To be exclusive to Horonobe, as many site-specific parameters were used as were available. The particle tracks supply the pathlengths and velocities. Pertinent parameters collected include porosity, saturation, density, half matrix block length, and temperature. The remaining parameter required to run STAMMT-L is the distribution coefficient, K_d – a parameter not yet measured for the media found near Horonobe. The STAMMT-L parameters were determined as follows:

The aqueous diffusion coefficient is calculated from the Stokes-Einstein equation (Bird et al., 1960, p. 513)

$$D_{aq} = \frac{kT}{3\pi\mu d}, \tag{11}$$

where $k = 1.38\times10^{-23}$ [M^{2}L/Kelvin] is Boltzmann's constant, T [Kelvin] is the absolute temperature of the interstitial water, d [L] is the nuclear radius of the radionuclide given in Table 3, and μ [M/LT] is the viscosity, which is an empirical function of temperature:

$$\mu(T) = 1.6\times10^{-2}\exp\left[-2.5\times10^{-2}\left(T-273.15\right)\right]. \tag{12}$$

Table 3: Nuclear radii for the radionuclides of interest at the Horonobe site studied here.

Element	Nuclear radius (Å)
Np	1,750
Th	1,800
U	1,750

An emperical relationship for tortuosity defined by Millington and Quirk (1960) is used in this analysis:

$$\tau = \frac{\theta^{\frac{7}{3}}}{\phi_{im}^2}, \tag{13}$$

where θ [M^3/M^3] is the degree of saturation.

To simplify this preliminary uncertainty and sensitivity analysis and to be conservative, it is assumed that there is no retardation in the mobile zone, which effectively stipulates that there is no sorption of radionuclides onto the fracture surfaces. Additionally, without any knowledge of the fracture fill at Horonobe, the mobile zone porosity is set to unity, $\phi_m = 1$.

Retardation is allowed in the immobile zone and is defined as

$$R_{im} = 1 + \frac{K_d \rho_b}{\phi_{im}}. \tag{14}$$

Although K_d has not been measured in Horonobe media, estimates of mean values have been provided in the JNC H12 report (JNC, 2000) as shown in Table 4.

Table 4: Reference mean distribution coefficients (JNC, 2000).

Element	K_d (m^3/kg)
Np	1
Th	1
U	1

Given (11), (12), (13), and (14), and the data presented in Table 3 and Table 4, there is sufficient information to formulate the capacity ratio and the diffusion rate coefficient. In reduced form, (4) can be rewritten in terms of measured or specified parameters (by substituting (14) and setting $R_{im} = \phi_{im} = 1$) as

$$\beta_{tot} = \phi_{im} + K_d \rho_b, \tag{15}$$

and, similarly, (5) becomes

$$\alpha_d = \frac{20.8kT\theta^{\frac{7}{3}}}{\pi \exp\left[-2.5\times10^{-2}\left(T-273.15\right)\right] d\phi_{im}\left(\phi_{im}+K_d\rho_b\right)\ell^2}. \tag{16}$$

Note that because the mean K_d and nuclear radius of Np, Th, and U are virtually equivalent, the modeling results presented here apply to all three equally. Future experimental data is expected to differentiate the transport properties of the three radionuclides and new sensitivity analyses should be conducted as updated data are made available.

Site Data

At HDB-1 and HDB-2, physical properties including porosity, saturation, density, and the number of fractures per meter were measured to depths of 720 m. Temperatures measured with depth collected at HDB-3, 4, and 5 are assumed applicable at HDB-1 and 2. The following sections detail the site data as well as the empirical or best fit CDF.

Half matrix block length - λ

For both HDB-1 and HDB-2, the number of fractures per meter of core, f [1/L], were physically counted and recorded. Throughout 720 m of drilling depth, 694 and 690 fracture counts were recorded at HDB-1 a HDB-2, respectively. Figure 3 shows the number of fractures counted per meter of core as a function of depth at HDB-1 and HDB-2. Note that there is some correlation with depth in each borehole with HDB-1 having fewer fractures per meter with increasing depth and HDB-2 having more fractures per meter as the core was drilled deeper. The number of fractures counted per meter and the corresponding empirical CDFs were created. Figure 4 shows both the empirical CDFs (symbols) and the analytical CDF (curves) used as the best match. A mathematical expression is used for these CDFs because of the close correlation between the emperical and analytical fit. The distribution of fractures per meter at HDB-1 is best approximated by a gamma distribution given by

$$F(x) = 1 - \int_{x}^{\infty} \frac{1}{\xi^{\zeta}\Gamma(\zeta)} x^{\zeta-1} \exp\left(-\frac{x}{\xi}\right) dx, \tag{17}$$

where Γ is the gamma function and the constants $\zeta = 0.43$ [–] and $\xi = 5.3$ [L] are fit with the least squares method. The distribution of fractures per meter at HDB-2 is best approximated by a triangular distribution given by

$$F(x) = 1 - \left(\frac{b-x}{b-a}\right)^2, \tag{18}$$

where minimum, a, and maximum, b, [1\L] are 0 and 33, respectively and are found with the least squares method.

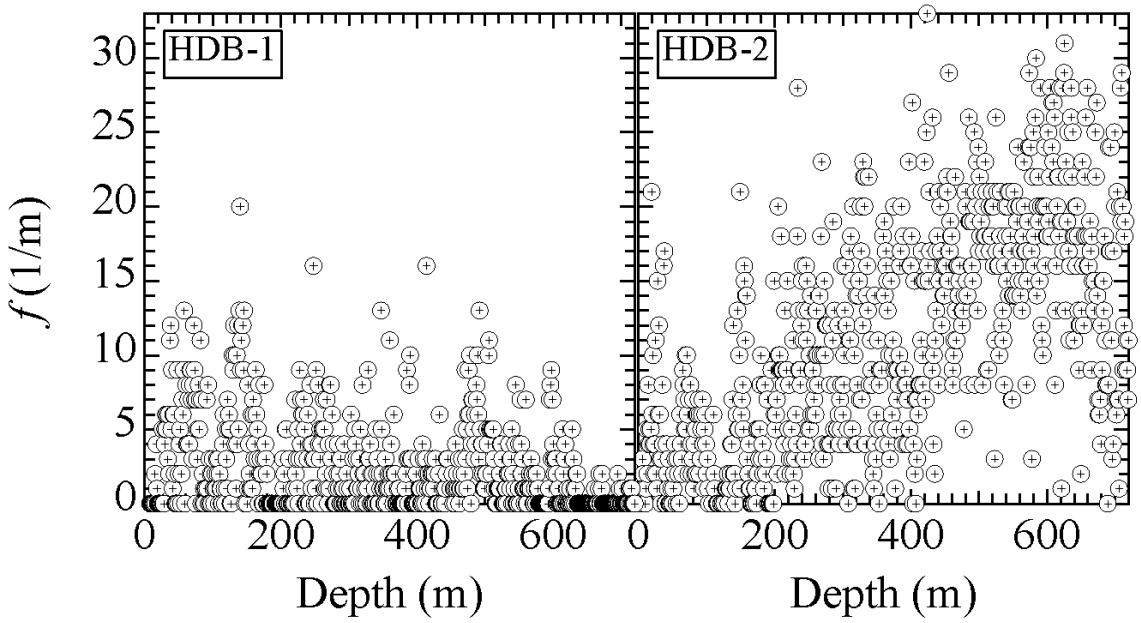

Figure 3: Number of fractures counted per meter at HDB-1 and HDB-2.

Once the number of fractures per meter is known, the half matrix block length was calculated as

$$\ell = \frac{0.5}{f}, \tag{19}$$

which is simply one-half divided by the number of fractures counted per meter. It should be noted that it is implicitly assumed that the fracture spacing is three-dimensional, even though the model is one-dimensional. Although it was often the case that no fractures were counted per meter, the empirical CDF was set to zero at a fracture frequency of 0 when fitting the distribution coefficients with the least squares method. This is a reasonable approximation because zero fractures per meter yields an undefined half matrix block length from (19), and because the probability of selecting exactly zero in a random drawing from (17) or (18) is zero. Furthermore, from LHS values, it is possible to select very small fracture frequencies. To avoid numerical complications that arise in these instances, as well as to accurately represent the geology, the half matrix block length is truncated at an upper limit of 2 m (one fracture every 4 m). This results in a conservative estimate for breakthrough because larger half matrix block lengths would yield

smaller mass transfer rates between mobile and immobile zones and therefore faster overall transport. This is because smaller matrix blocks reach equilibrium more quickly with the fluid in the fractures than larger matrix blocks.

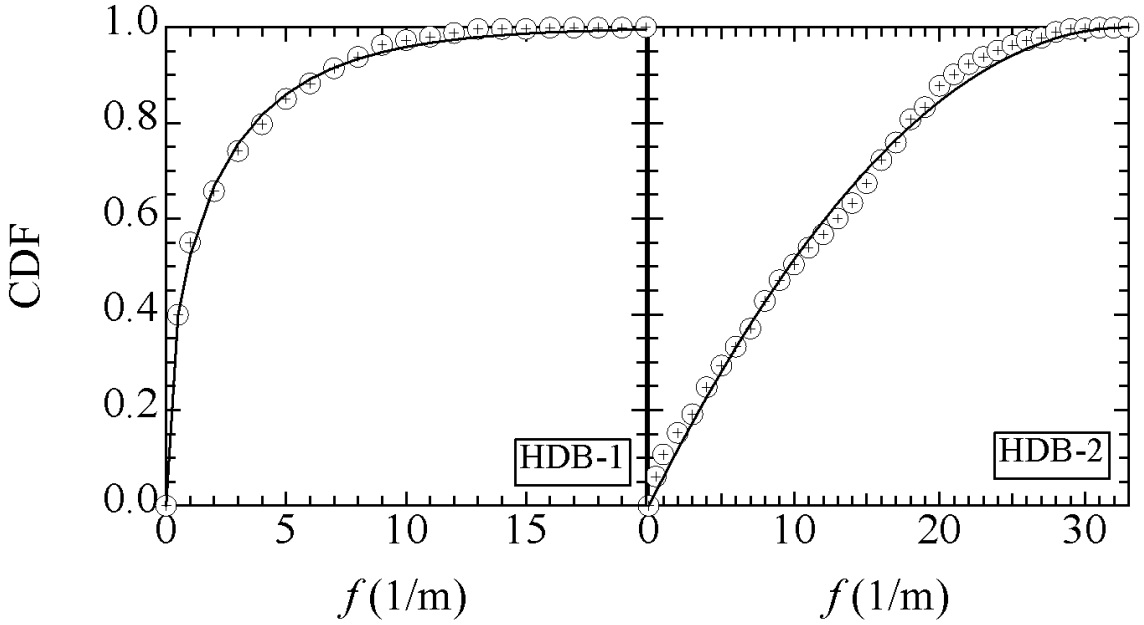

Figure 4: Empirical and analytical CDF approximation used for the number of fractures per meter at HDB-1 and HDB-2. HDB-1 is best represented by a gamma distribution and HDB-2 is best represented by a triangular distribution.

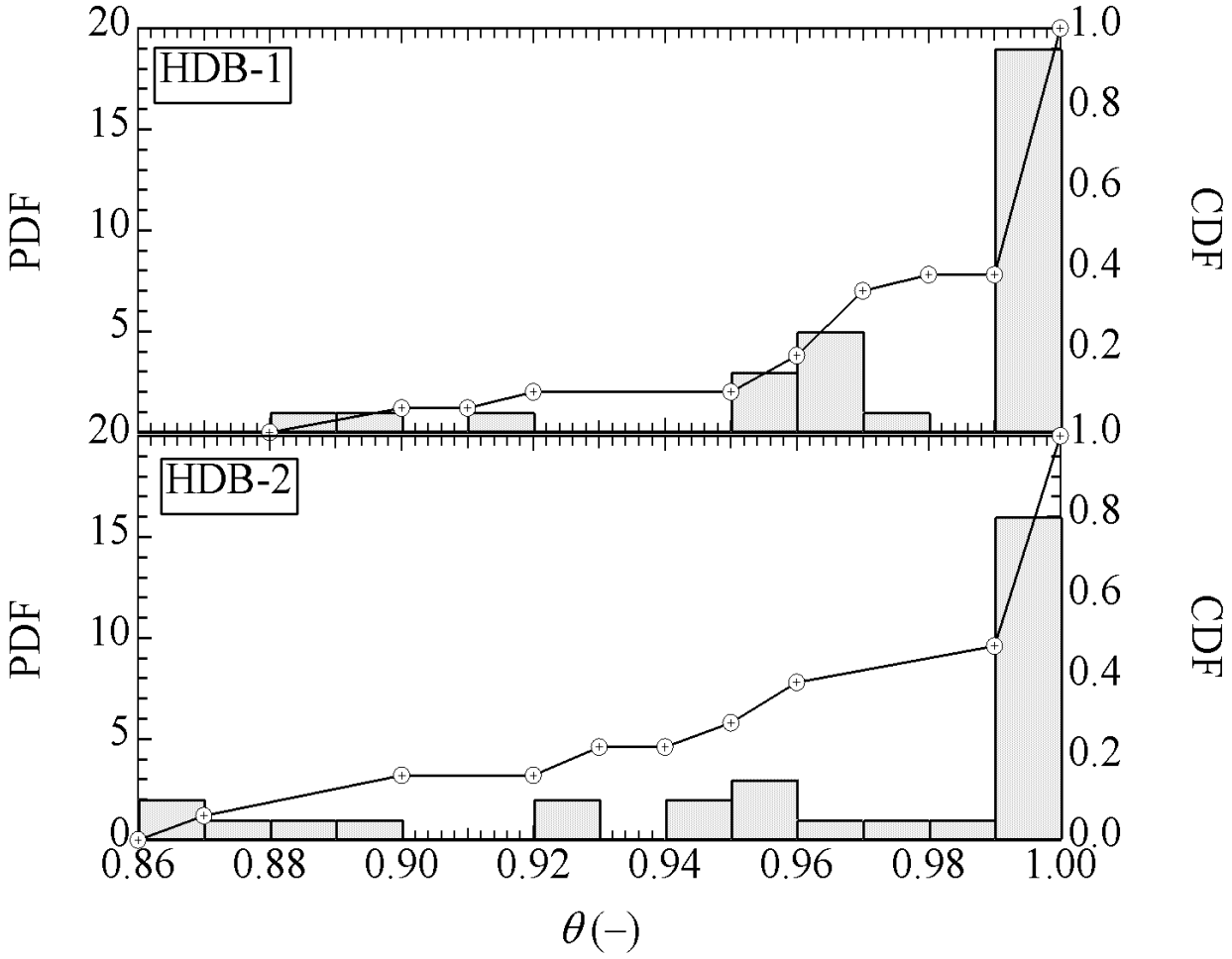

Figure 5: Probability density and cumulative distribution functions for saturations at HDB-1 and HDB-2.

Saturation - θ

The water table at Horonobe is very near to the surface and the in the flow model it is assumed that saturated conditions exist everywhere. Nevertheless, saturation measurements were taken and thus will be considered in this analysis. Saturations were always greater than 86% and their distributions along with their corresponding piecewise linear CDFs are presented in Figure 5.

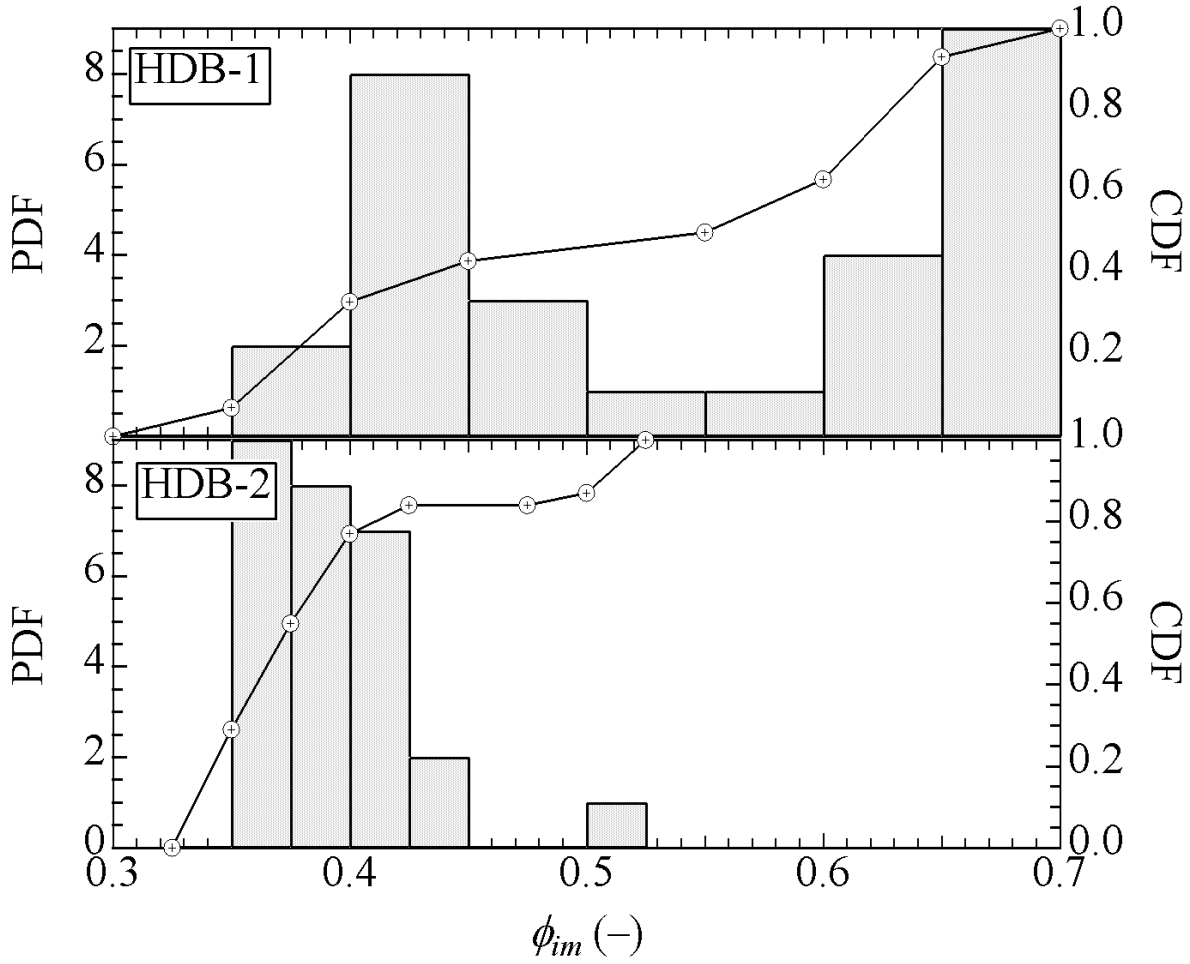

Figure 6: Probability density and cumulative distribution functions for porosities at HDB-1 and HDB-2.

Porosity - ϕ_{im}

Although porosity was fixed at 0.38 in the flow model, for the STAMMT-L transport calculations it is a randomly sampled input parameter. Porosities were measured with depth and the corresponding probability densities (PDFs) and CDFs are shown in Figure 6. Note that because of the spread of the data, the histogram bins for HDB-1 are twice as wide as those selected for HDB-2. Note also that the media at HDB-1 prove to be more porous, in general, than those at HDB-2.

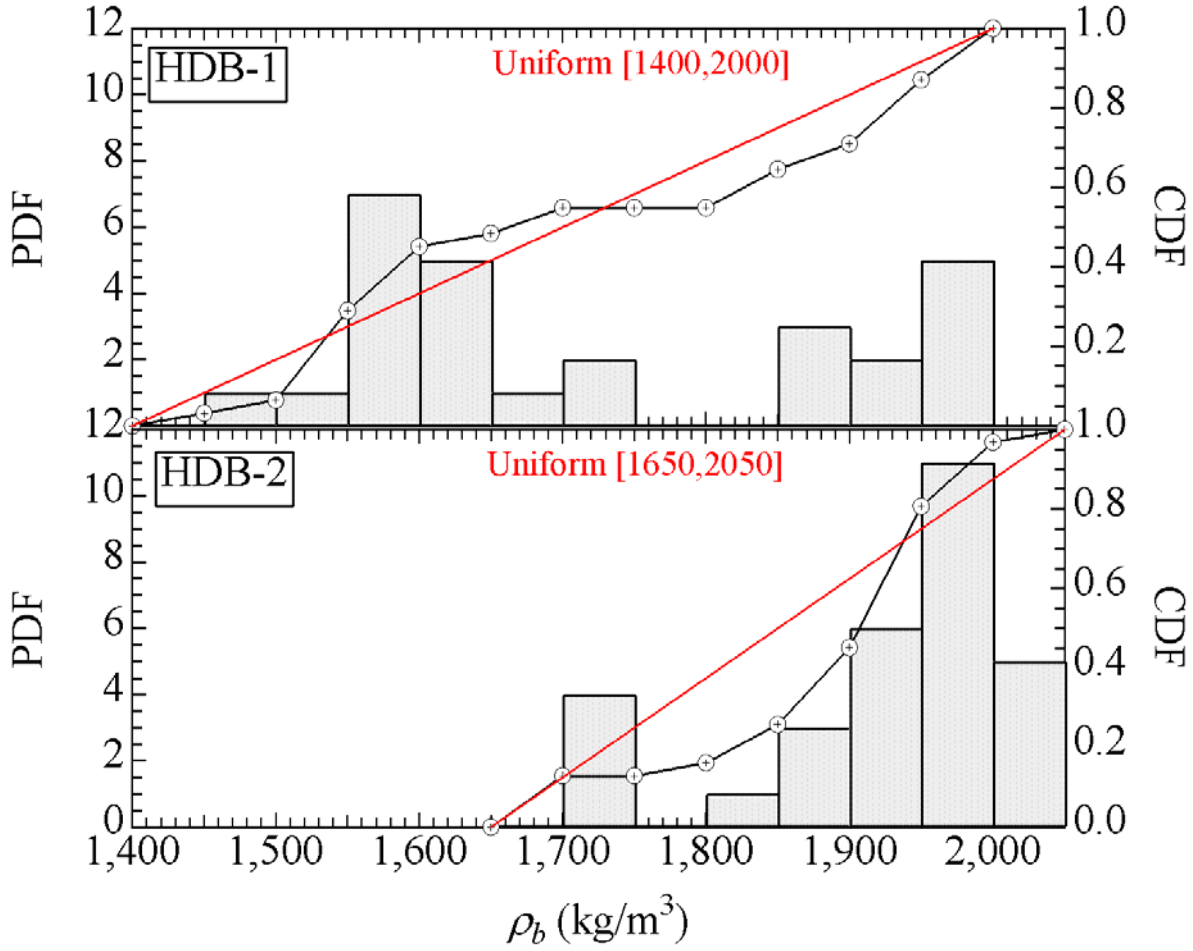

Figure 7: Probability density and cumulative distribution functions for densities at HDB-1 and HDB-2 and the corresponding uniform distribution used to represent the data.

Density - ρ_b

Density was measured with depth and the corresponding PDFs and CDFs are shown in Figure 7. They appear to be well approximated by uniform distributions as indicated by the red CDF lines in the figure. The paucity of data in this case warrants a linear fit. At HDB-1 densities range from 1,400 to 2,000 kg/m3 and at HDB-2 they range from 1,650 to 2,050 kg/m^3. Corresponding to the lower porosities found at HDB-2 compared to HDB-1, the densities at HDB-2 are greater than those at HDB-1.

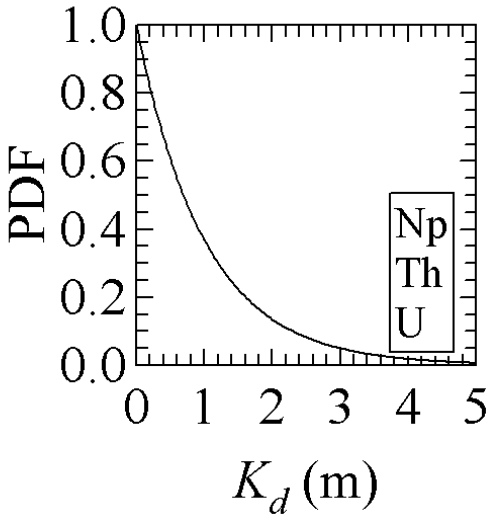

Figure 8: Exponential probability density for K_d with mean 1.

Distribution coefficient - K_d

Although no distribution coefficients have been measured at the Horonobe site, Table 4 lists reference values for the radionuclides of interest. Exponential distributions with mean set to the value in Table 4 are used for Np, Th, and U as shown in Figure 8. This ensures that many small values for K_d will be selected. Without knowing any further site information, this is a reasonably conservative selection for a distribution because radionuclide transport will be fastest (least retarded) for those with the smallest K_d and the median distribution coefficient is less than the mean. Although the exponential distribution has no upper bound, the largest K_d selected by the LHS program was 6.2

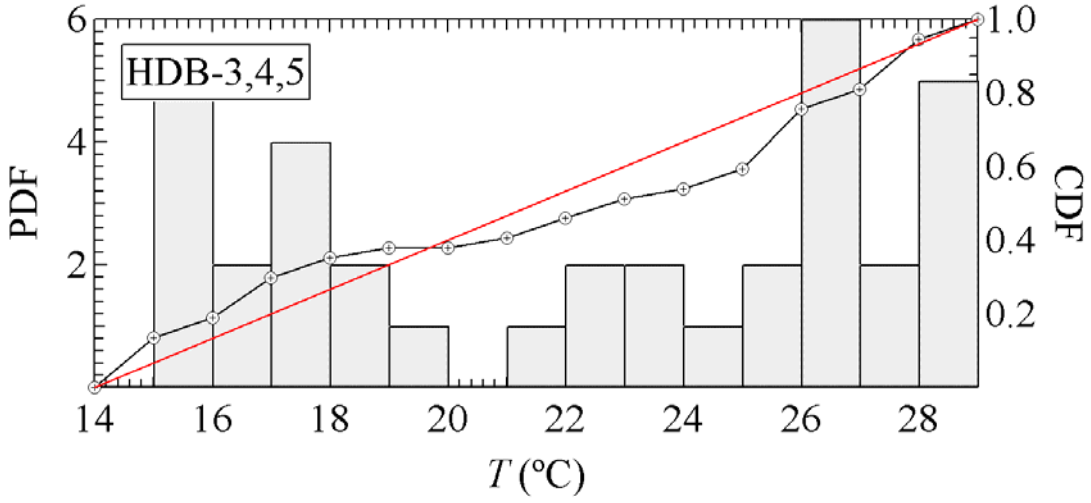

Figure 9: Distribution of temperatures measured at HDB-3, HDB-4, and HDB-5. The red line (uniform between 14 and 29) approximates the measured distribution.

Temperature – *T*

The distribution of temperatures recoded at HDB-3, HDB-4, and HDB-5 are shown in Figure 9. The measured distribution is well approximated by a uniform distribution between 14 and 29°C as illustrated with the red line.

Correlations

Using Microsoft Excel™, correlation coefficients were calculated for each measured site parameter with depth. As all parameters are correlated with depth, it is possible to cross correlate them. Table 6 shows the correlation coefficient for each of the parameters with depth. The text within the table is color coded to indicate which borehole the data correlations are applicable. Note the strong correlation between temperature and density and the strong inverse correlation between density and porosity. All are related through their high correlations with depth. This indicates that as overburden pressure increases, porosity decreases and density increases nearly proportionally. This also indicates that the medium is fairly homogeneous and that there are no large transitions between types of geologic units. Furthermore, the strong correlation of temperature with depth indicates that there is an increasing thermal gradient of about 0.04°C per meter of depth.

Table 5: Correlation coefficients between all measured site data (blue entries are for HDB-1 and red entries are for HDB-2).

	depth	ρ_b	ϕ_{im}	θ	*T*	*f*
depth	1	**0.53**	**–0.58**	**0.10**	**0.99**	**0.56**
ρ_b	**0.94**	1	**–0.97**	**–0.22**	**–0.64**	**0.26**
ϕ_{im}	**–0.94**	**–0.99**	1	**0.27**	**0.49**	**–0.36**
θ	**–0.25**	**–0.25**	**0.32**	1	**0.34**	**–0.12**
T	**0.96**	**0.93**	**-0.91**	**0.02**	1	**0.31**
f	**–0.28**	**–0.28**	**0.30**	**–0.09**	**0.29**	1

Stochastic transport simulations

The LHS code was used to generate 3,744 sets of parameter values for each particle track, yielding 63,648 input vectors (17 particle tracks × 3,744 LHS vectors). The value of 3,744 LHS samples was selected because it ensured a sufficiently low variance in results (and was the maximum number handled by the stepwise linear regression program). Recall that 17 (base plus 16 variants, two for each change to a geologic unit) particle tracks were run to examine how changes in hydraulic conductivity altered path length and travel time. Hydraulic conductivity can be included as an independent parameter by supplying its value (base, low, and high) to ⅓ of the vectors (1,248) that coincide to the base and each variant case (including associated path lengths and velocities) and subsequently running stepwise linear regression (discussed below) over all vectors.

STAMMT-L was run with a batch file such that a breakthrough curve was generated for each of the 3,744 vectors for each particle track. An example of 100 breakthrough curves is shown in Figure 10. Variation in the breakthrough curves is due to the range of values that are generated from the LHS variables. Note that some breakthrough curves have a long tail, this is likely a result of a combination of parameters that results in a high mass transfer rate, α_d, and a large capacity, β_{tot}. As a metric for the sensitivity analysis, the 5%, 50%, and 95% breakthrough times were linearly interpolated from each breakthrough curve and used to define cumulative distributions. The 5%, 50%, and 95% breakthrough times correspond to the times when the normalized concentration at the observation location equaled 0.05, 0.5, and 0.95, respectively. These cumulative distributions represent the range of 5%, 50%, and 95% breakthrough times due to the uncertainty in the input parameters. Recall that a wider range in uncertainty of the input parameters corresponds to a wider range of breakthrough times.

The cumulative distributions for the 5% (green), 50% (red), and 95% (blue) breakthrough times for the two sources studied applicable to Np, Th, or U are shown in Figure 11. Particles released at HDB-1 are shown with the solid curves, and particles released at HDB-2 are represented with broken curves. The 'stair-stepping' of the CDFs for HDB-2 could be artifacts of the three distinct values of hydraulic conductivity. The cumulative distributions are presented for each variant as noted by the letter in the bottom right of each plot that corresponds to Table 1.

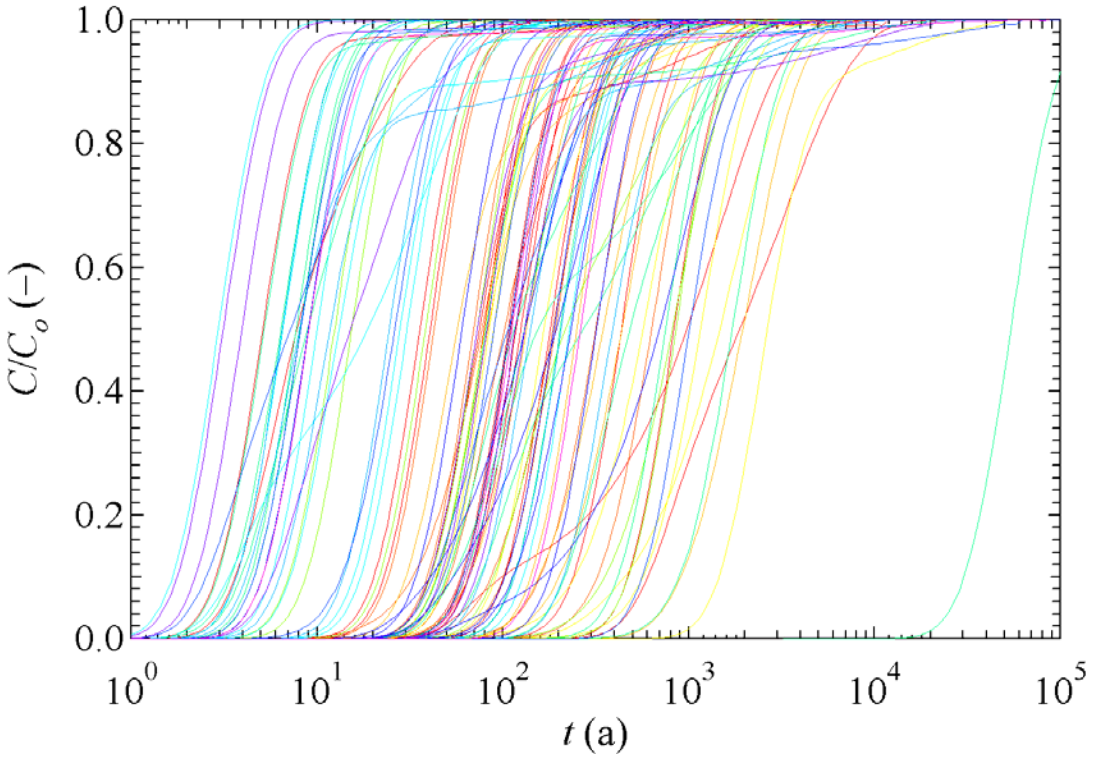

Figure 10: STAMMT-L breakthrough curves using 100 realizations of LHS parameters.

Stepwise Linear Regression

Stepwise linear regression is a regression analysis technique used to assess parameter sensitivities. A code called STEPWISE (WIPP, 1995) was used to perform various statistical analyses to assess sensitivities to input variables of breakthrough results calculated by STAMMT-L. The code was further developed by Iman et al. (1980) and has since served as a regression-

analysis code within Sandia National Laboratories. Rank transformation is used to correlate the parameters (i.e., the parameters are sorted in ascending order and their ranks are used to calculate correlations). A complex hydrological model employs many geophysical variables whose numerical values are known with varying degrees of certainty. Understandably, parameters with values have a strong influence on breakthrough results are of greater concern and STEPWISE is used to identify them and quantify the strength of their influence. The stepwise regression procedure uses the forward regression procedure, which begins by regressing on the one independent variable in the model that explains the most variation in the dependent variable, as measured by its having the largest sample correlation coefficient with the dependent variable (breakthrough time). At each step of the analysis, the variables presently in the regression model are reexamined regarding their current contribution to the regression sum of squares. The variable contributing least to the regression is dropped from the analysis, providing its contribution is below a user-specified level of significance. This procedure continues until only variables that are significant above some prespecified level remain in the model.

Using the calculated 5%, 50%, and 95% breakthrough times as the dependent variables, STEPWISE was run for each variant to ascertain which of the site parameters most influenced transport time. The coefficient of determination is used to describe a parameter's sensitivity and it is the percent of the dependent parameter variation that can be explained by the regression equation (or the explained variation divided by the total variation). Table 6 lists the coefficients of determination averages over all variants for each variable at the 5%, 50%, and 95% breakthrough times. In addition, the overall average is also presented.

Table 6: Coefficients of determination, Δr^2, for the STAMMT-L input variables.

Breakthrough	K_d	K	λ	T	θ	ρ_b	ϕ_{im}	Sum
5%	0.189	0.138	0.031	0.016	0.004	0.005	0.006	0.389
50%	0.375	0.107	0.006	0.008	0.003	0.004	0.004	0.507
95%	0.700	0.088	0.001	0.005	0.001	0.002	0.001	0.798
Average	0.421	0.124	0.017	0.011	0.005	0.005	0.004	0.587

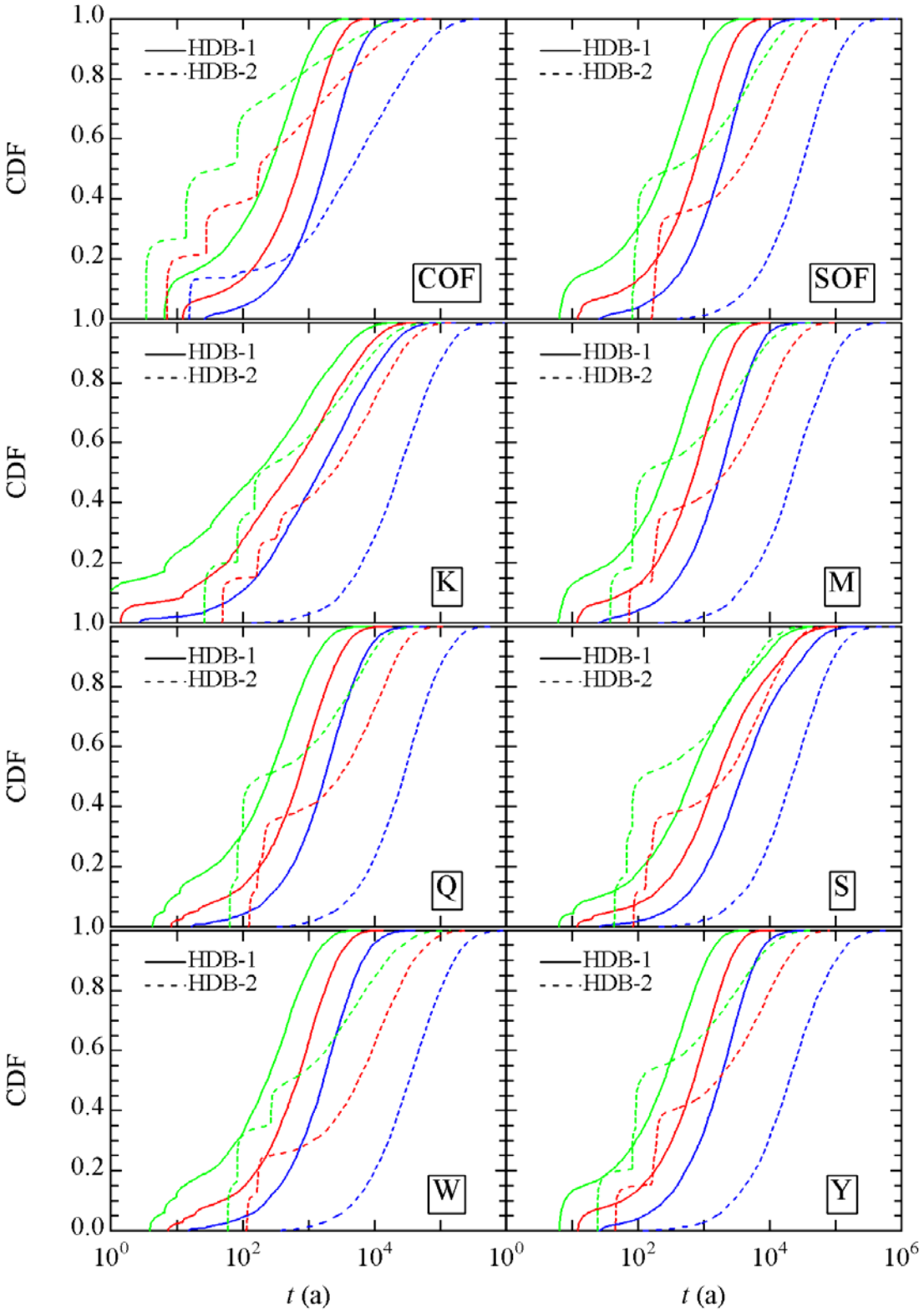

Figure 11: Cumulative distributions of 5% (green), 50% (red), and 95% (blue) breakthrough times for each variant (as noted in the box in the lower left of each plot) for particles released at HDB-1 (solid) and HDB-2 (dashed).

Discussion

It is instructive to examine a selected subset of LHS vectors and their impacts on the dependent variable, breakthrough time. Figure 12 shows the scatter plots of the Koitoi (**K**, see Table 1) variants for a particle released at HDB-2 with the 95% breakthrough time as the dependent metric. This clearly shows the correlations between the input parameters, which may be read by the looking for the intersection of one row of a parameter with the column of another. In addition, the slope of the red line in the figure is the calculated correlation coefficient, which should be quite close to the corresponding specified correlation coefficient in Table 5. Note that the hydraulic conductivity is not correlated with any other input variables (slope of red line is zero) and that the three columns or rows represent the three variants – base, low, and high. Finally, the correlation of the model parameters with the breakthrough time can be noted in the last column (or bottom row) where the red line indicates how changes in the independent variable affect the breakthrough time. Figure 12 and Table 6 indicate that K_d is the most important variable with K next most important.

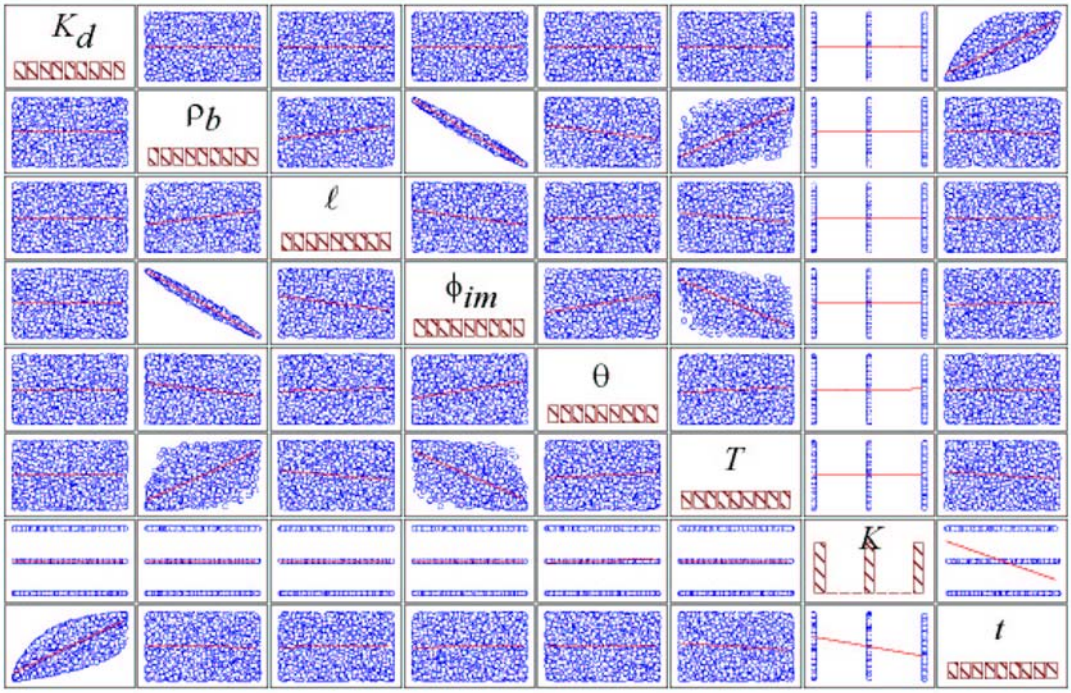

Figure 12: Correlation analysis of all independent and the dependent parameters for the 95% breakthrough time for K variant. The red lines indicate the correlation coefficient.

The cumulative distributions of travel times reveal several noteworthy characteristics. For example, Figure 13 is an overlay of the cumulative distributions for the 5, 50, and 95% breakthrough times for the **COF**, **SOF**, **M**, and **Y** variants for particles released at HDB-1. Note that they are virtually identical indicating that the particle tracks are not affected by changes in hydraulic conductivity of these formations and thus the particle tracks do not pass through these formations. Although for HDB-2 there are no variants that exactly overlap, this does not necessarily imply that the particles pass through each geologic unit. Because the flow field of the entire model is everywhere impacted to some degree by a change in hydraulic conductivity of a single geologic unit, particle tracks can be affected even if they do not pass through the variant geologic unit. For example, Figure 14 shows the cumulative distributions for the 5%, 50%, and

95% breakthrough times for the **M** and **Y** variants for particles released at HDB-2. Because they are so similar, it is likely that the particles do not pass through these formations, but their paths are altered slightly because of changes in the global flow field due to changes in hydraulic conductivities of the Mashuhoro and Yuuchi formations. With 3,744 input vectors, it is unlikely that variations in the LHS values could account for the differences shown in Figure 14.

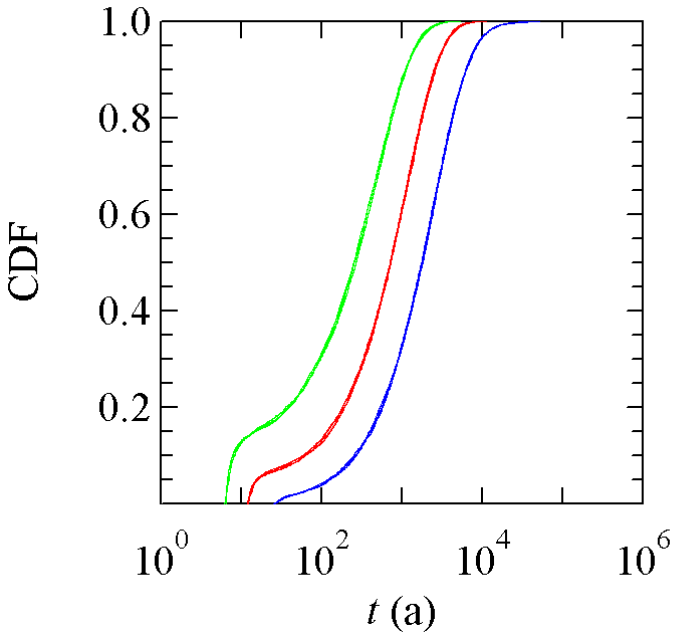

Figure 13: Cumulative distributions of the 5%, 50%, and 95% breakthrough times for particles from HDB-1 for variants COF, SOF, M, and Y.

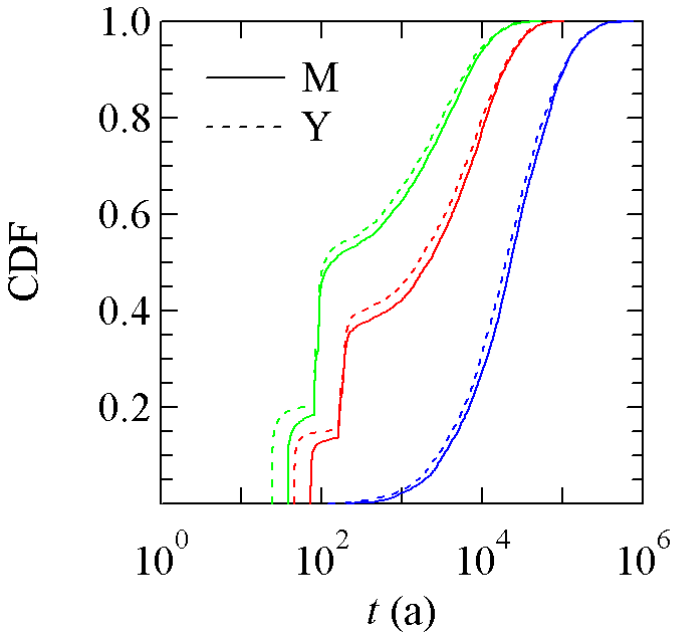

Figure 14: Cumulative distributions of the 5%, 50%, and 95% breakthrough times for particles from HDB-2 for variants M (solid curves) and Y (dashed curves).

Upon examination of the cumulative distributions for the 5%, 50%, and 95% breakthrough times for the **COF** and **SOF** variants for particles released at HDB-2, it is clear that the particles are strongly influenced by changes in hydraulic conductivities of these features (see Figure 15). This indicates that particles released from HDB-2 pass through the low conductivity Oomagari Fault.

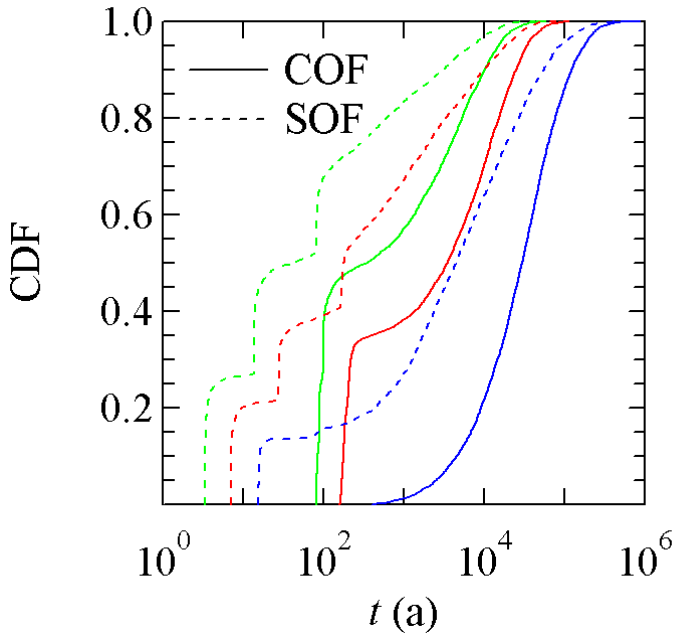

Figure 15: Cumulative distributions of the 5%, 50%, and 95% breakthrough times for particles from HDB-2 for variants COF (solid curves) and SOF (dashed curves).

Several observations are made about the coefficients of determination for the input variables:

- With respect to the overall average coefficients of determination, the ranking of variables in order of importance is K_d, K, λ, T, θ, ρ_b, and ϕ_{im};
- All parameters decrease in importance with increasing breakthrough times (read down a column of Table 6) except for K_d, which sharply increases in importance; and,
- The sums of the coefficients of determination increase with increasing breakthrough time.

It is not surprising that K_d becomes a more important parameter at late times because the longer a sorbing radionuclide stays in the media due to matrix diffusion, the more its transport is delayed due to retardation. Therefore, late-time arrival is dominated by the distribution coefficient. The other parameters are more important at early times because values on either end of the distribution (depending on the parameter) can play a strong role in the early time radionuclide arrival. For example, for vectors with large λ, the mass transfer rate, a retarding mechanism, is significantly slowed (see (16)) and earlier breakthrough is expected

It is somewhat surprising that the sums of the coefficients of determination are always below 0.8, however several possible explanations exist. For example, as shown in Figure 13, several variants are unaffected by changes in hydraulic conductivity. The averaging process tends to dilute the sensitivity of this variable because, for some variants (Figure 15), it is the most important parameter, and for others its impact is negligible. In addition, it is known that high correlation coefficients among the input parameters complicate the stepwise linear regression process and, as shown in Table 5, there are several strong correlations (i.e., with magnitudes greater than 0.7). Furthermore, linear interpolation used to calculate the 5%, 50%, and 95% breakthrough times

form the log-uniformly spaced STAMMT-L output times introduces some approximation error, which could decrease the overall coefficient of determination. Finally, there is the possibility that oscillations are introduced by the IMSL routine used to perform the inverse Laplace transform of the transport equation (DINLAP) because a truncated Taylor series is used to approximate the solution.

It is perhaps unexpected that the temperature has a higher average coefficient of determination than θ, ρ_b, and ϕ_{im} although the strong correlation between T, ρ_b, and ϕ_{im} may incorrectly attribute the importance of ρ_b, and ϕ_{im} to T. Nevertheless, all parameters other than K_d and K affect breakthrough times only slightly.

Conclusions

Because this uncertainty and sensitivity analysis is specific to the conceptual models used (i.e., the flow model and STAMMT-L), it must be emphasized that the conceptual model could be the most important factor in the analysis and that using different models (or even implementing the hydraulic conductivity differently) could yield significantly different results. This analysis used LHS to select random transport parameters for input to the semi-analytical, one-dimensional, multirate transport model, STAMMT-L, yielding the 5%, 50%, and 95% breakthrough times that are used as the sensitivity metric (dependent variable). Particle path lengths and travel times are derived from the finite element flow and particle tracking model. Cumulative distributions of 5%, 50%, and 95% breakthrough times indicate that for the range of uncertainty in the input parameters, breakthrough times can span more than three orders of magnitude. The parameters controlling breakthrough time are K_d and K, and to a lesser extent, ℓ. At this point in the research and development of the Horonobe URL, it is clear that it is these most important parameters that need to be further studied and measured. Future work could focus on identifying appropriate distribution coefficients for each radionuclide of interest as well as determining the hydrological and chemical parameters of the geology on a per unit basis. Furthermore, full distributions for K_d should be developed so that modelers do not have to rely on mid and end member values.

Conclusions that can be drawn from this analysis are that:

1) the distribution coefficient needs to be characterized at the site;
2) more unit specific information needs to be gathered (e.g., does the fracture frequency change between geologic units?);
3) a distribution of hydraulic conductivities for each unit should be specified and used in a separate flow model (e.g., MODFLOW); and,
4) sufficient data exist to preliminarily determine the correlation of depth with temperature, porosity, and density; however, more data are always useful.

References

Bird, R. B., W. E. Stewart, and E. N. Lightfoot, *Transport phenomenon*, Wiley, New York, 1960.

BGS, Mineralogical observations and interpretation of porewater chemistry from Horonobe deep boreholes HDB1 and HDB2, Hokkaido, Japan, Commercial Report CR/02/303, 2002.

Haggerty, R. S., Application of the multirate diffusion approach in tracer test studies at Äspö HRL, SKB Report 99-62, 1999.

Haggerty, R. S., S. W. Fleming, L. C. Meigs, and S. A. McKenna, Tracer tests in a fractured dolomite 2. Analysis of mass transfer in single-well injection-withdrawal tests, *Water Resour. Res*., 37(5), 1129–1142, 2001

Haggerty, R. and S. M. Gorelick, Multiple-rate mass transfer for modeling diffusion and surface reactions in media with pore-scale heterogeneity, *Water Resour. Res*., 31(10), 2383-2400, 1995.

Haggerty, R. and S. M. Gorelick, Modeling mass transfer processes in soil columns with pore-scale heterogeneity. *Soil Sci. Soc. Am J*., 62(1), 62-74, 1998.

Haggerty, R. and P. Reeves, STAMMT-L: Solute Transport and Multirate Mass Transfer, User's Manual. Sandia National Laboratories, NM, 1999.

JNC, H12: Project to establish the scientific and technical basis for HLW disposal in Japan, Supporting Report 3: Safety assessment of the geological disposal system, JNC TN1410 2000-004, 2000.

JNC, Study on Regional Groundwater Flow Analysis Relevant to the Horonobe Underground Research Program, JNC Technical Report (Document Prepared by Hazama Corporation, Based on the Trust Contract), JNC TJ1400, 2002 (in Japanese).

Iman, R. L., J. M. Davenport, E. L. Frost, and M. J. Shortencarier, *Stepwise Regression with PRESS and Rank Regression* (*Program User's Guide*). SAND79-1472. Sandia National Laboratories, NM, 1980.

McKenna, S. A., Solute transport modeling of the Äspö STT-1b tracer tests with multiple rates of mass transfer, Task 4E: Äspö Task Force on Modelling of Groundwater Flow and Transport of Solutes, SKB-ICR-99-02, SKB, 1999.

McKenna, S. A., Prediction of STT-2 tracer tests: Application of the multirate model, SAND2000-2190C, Sandia National Laboratories, NM, 2000a.

McKenna, S.A., Solute transport modeling of the Äspö STT-1b tracer test with multiple rates of mass transfer, SAND2000-2189C, Sandia National Laboratories, NM, 2000b.

McKenna, S. A., L. C. Meigs, and R. Haggerty, Tracer tests in a fractured dolomite 3. Double-porosity, multiple-rate mass transfer processes in convergent flow tracer tests. *Water Resour. Res*., 37(5), 1143-1154, 2001.

Meigs, L. C. R. L. Beauheim, and T. L. Jones, Interpretations of tracer tests performed in Culebra dolomite at the Waste Isolation Pilot Plant, SAND97-3109, Sandia National Laboratories, NM, 1997.

Millington, R.J. and J. P. Quirk, Permeability of porous solids, *Nature*, 57(8), 1200-1207, 1960.

WIPP, User's Manual for STEPWISE, Version 2.20, WPO#27768, Sandia National Laboratories, NM, 1995.

Distribution

FOREIGN DISTRIBUTION:

Richard Jensen
4-33, Muramatsu, Tokai-Mura, Naka-Gun
Ibaraki, Japan 319-1194

Takanori Kunimaru
Miyazono-machi 1-8, Horonobe-cho,
Hokkaido, Japan 098-3207

Hiroshi Kurikami
Miyazono-machi 1-8, Horonobe-cho
Hokkaido, Japan 098-3207

Hitoshi Makino (5)
4-33, Muramatsu, Tokai-Mura, Naka-Gun
Ibaraki, Japan 319-1194

Keiichiro Wakasugi (2)
4-33, Muramatsu, Tokai-Mura, Naka-Gun
Ibaraki, Japan 319-1194

Shinichi Yamasaki (2)
Miyazono-machi 1-8, Horonobe-cho
Hokkaido, Japan 098-3207

Mikazu Yui
4-33, Muramatsu, Tokai-Mura, Naka-Gun
Ibaraki, Japan 319-1194

SANDIA INTERNAL:

1	MS 0719	6142	S. M. Howarth
1	MS 0735	6115	S. J. Altman
1	MS 0735	6115	R. E. Finley
4	MS 0735	6115	S. C. James
1	MS 0735	6115	T. S. Lowry
1	MS 0735	6115	S. A. McKenna
1	MS 0778	6852	B. W. Arnold
2	MS 0899	9616	Technical Library
1	MS 9018	8945-1	Central Technical Files
1	MS 1393	12100	E. K. Webb